Available online at www.sciencedirect.com
SCIENCE DIRECT®
Journal of Power Sources 144 (2005) 141–145
JOURNAL OF POWER SOURCES
www.elsevier.com/locate/jpowsour

Short communication

Development of micro direct methanol fuel cells for high power applications

G.Q. Lu, C.Y. Wang*

Electrochemical Engine Center (ECEC), Department of Mechanical and Nuclear Engineering, The Pennsylvania State University, University Park, PA 16802, USA

Received 17 November 2004; received in revised form 19 December 2004; accepted 19 December 2004
Available online 15 February 2005

Abstract

A micro direct methanol fuel cell (μDMFC) with active area of 1.625 cm^2 has been developed for high power portable applications and its electrochemical characterization carried out in this study. The fragility of the silicon wafer makes it difficult to compress the cell for good sealing and hence to reduce contact resistance in the Si-based μDMFC. We have instead used very thin stainless steel plates as bipolar plates with the flow field machined by photochemical etching technology. For both anode and cathode flow fields, widths of both the channel and rib were 750 μm, with a channel depth of 500 μm. A gold layer was deposited on the stainless steel plate to prevent corrosion. This study used an advanced MEA developed in-house featuring a modified anode backing structure with a compact microporous layer. Maximum power density of the micro DMFC reached 62.5 mW cm^{-2} at 40 °C, and 100 mW cm^{-2} at 60 °C at atmospheric pressure, which almost doubled the performance of our previous Si-based μDMFC.

Keywords: DMFC; Micro fuel cell; High power

1. Introduction

The direct methanol fuel cell (DMFC) is a promising power source for portable applications due to advantages such as simple construction, compact design, high energy density, and relatively high energy-conversion efficiency [1–7]. For high power applications such as laptop computers, PDAs and camcorders, it is necessary to enhance the cell performance further in order to compete with the lithium ion battery.

To date, most micro DMFCs (μDMFC) and proton exchange membrane fuel cells (PEMFCs) were developed based on microelectromechanical system (MEMS) technology [6–16]. Kelley et al. reported a 0.25 cm^2 micro DMFC [8] and subsequently a prototype cell (12 mm^3 in volume) micro-fabricated on Si substrates [9]. Recently, Lu et al. also reported a Si-based micro direct methanol fuel cell [6,7].

A problem emerging in micro fuel cells based on Si wafer is that the Si substrate is quite fragile, making difficult to compress the fuel cell tightly for good seals and for lowering the contact resistance between MEA and Si-based bipolar plates. Pavio et al. instead explored low-temperature co-fired ceramic (LTCC) material as an alternative for the bipolar plate of micro fuel cell systems, and a DMFC prototype, packaged using LTCC, was reported [17]. However, both silicon wafer and ceramic are nearly electrically insulated. Conductivity for current collection fully depends on the thickness of the conductive layer coated on these substrates, which will increase the cost significantly in order to minimize the resistance required in high power application.

An alternative method to fabricate the bipolar plate is proposed in this paper using photochemical etching of thin stainless steel plates (500 μm or thinner) for μDMFCs instead of silicon wafer and ceramic. Stainless steel has much higher conductivity and mechanical strength. A thin layer of gold coating on stainless steel plate is sufficient to prevent

* Corresponding author. Tel.: +1 814 863 4762; fax: +1 814 863 4848.
E-mail address: cxw31@psu.edu (C.Y. Wang).

0378-7753/$ – see front matter © 2005 Elsevier B.V. All rights reserved.
doi:10.1016/j.jpowsour.2004.12.023

corrosion and improve the electrical contact. Photochemical etching is a high-quality, fast-turnaround, low-cost method for machining flat metal parts. For micro-fabrication of flow channels in the stainless steel bipolar plate, it offers precision and accuracy unavailable in other milling processes.

In this paper, a μDMFC fabricated by photochemical etching has been developed, with an effective area of 1.625 cm^2, and with the same flow pattern and effective area as the Si-based micro DMFC we reported earlier [6]. The advanced MEA developed in-house for use in this study has a modified anode backing structure with a compact microporous layer. Nafion® 112 membrane was used in the MEA. The μDMFC is subsequently tested and the maximum power density reaches 62.5 mW cm^{-2} at 40 °C and 100 mW cm^{-2} at 60 °C with atmospheric pressure.

2. Experimental

Stainless steel plates with thickness of 500 μm have been used as bipolar plates for current collection and flow distribution. The flow channels were photochemically etched in the stainless steel plates, and the flow pattern was same as the Si-based μDMFC we reported earlier [6]. Both the flow channel and the rib separating two neighboring channels were 750 μm wide, with a channel length of 12.75 mm. There were a total of nine channels with serpentine flow-field, forming a cell with an effective area of approximately 1.625 cm^2. In order to minimize contact resistance between the MEA and the substrate, a gold layer with thickness of 0.5 μm was deposited on the front side of each stainless steel plate. In this paper, we focus our main interest on gross cell performance without paying attention to the size and input power for accessory parts. Further optimization of the system to minimize the auxiliary power and the cell volume to yield high net power density is undergoing and the results will be reported in a future publication.

2.1. MEA preparation

Both backing layers of anode and cathode were 30 wt.% FEP wet-proofed carbon paper (Toray 090, E-Tek) of 0.26 mm in thickness. Our approach to make a more methanol-resistant MEA is to add a compact microporous layer in the anode structure by providing additional resistance to methanol transport. Details of this approach have been elaborated in [18,6] and the reader is referred to those papers for further information. The catalyst for the anode was unsupported Pt/Ru black (HiSPEC 6000, Pt:Ru, 1:1 atomic ratio, Alfa Aesar), and the loadings of Pt/Ru and Nafion in the anode catalyst layer were 4.8 and 1.2 mg cm^{-2}, respectively. The catalyst for the cathode was carbon-supported Pt (40 wt.% Pt on Vulcan XC72R, E-Tek), and loadings of Pt and Nafion in the cathode catalyst layer were 1.8 and 1.35 mg cm^{-2}, respectively. Pretreated Nafion® 112 (EW 1100, Dupont) sandwiched by the catalyzed anode and cathode diffusion media, having the active area of 1.625 cm^2, was hot pressed at 125 °C and 100 kg cm^{-2} for 3 min to form an MEA.

2.2. Test apparatus

Methanol aqueous solution was prepared from 1 to 4 M to test the cell performance. A peristaltic pump was used to deliver the liquid fuel and the flow rate was obtained by weighing the fuel delivered per minute. A gas flow meter was used to measure the flow rate of non-preheated and non-humidified air. To investigate the cell characteristics at different temperatures, an electric heater with temperature controller was attached on the surface of the cell. An electronic load system (BT4, Arbin) in the galvanodynamic polarization mode was used to measure polarization curve at a scan rate of 3 mA s^{-1}.

3. Results and discussion

Fig. 1 shows the polarization curve and power density using 2 M methanol solution at 22 °C and atmospheric pressure. The methanol flow rate is 2.2 mL min^{-1}, and the air flow rate is 161 mL min^{-1}. The polarization curve was measured after the cell stablized at the open circuit voltage (OCV) for about 20 min. As expected, methanol kinetic is much more sluggish at room temperature and pressure, and the voltage decreases very quickly in the kinetic region of the polarization curve. The current density reaches 90 mA cm^{-2} at 0.3 V and the maximum power density is 34 mW cm^{-2} at 0.23 V. This is much better than our previous results using Si-based μDMFC where the maximum power density at 23 °C and atmospheric pressure was 16.5 mW cm^{-2} at 0.14 V [6]. The fact that the maximum power density is doubled as compared to the previous result is due largely to better compression, and thus, lower contact resistance between the MEA and SS bipo-

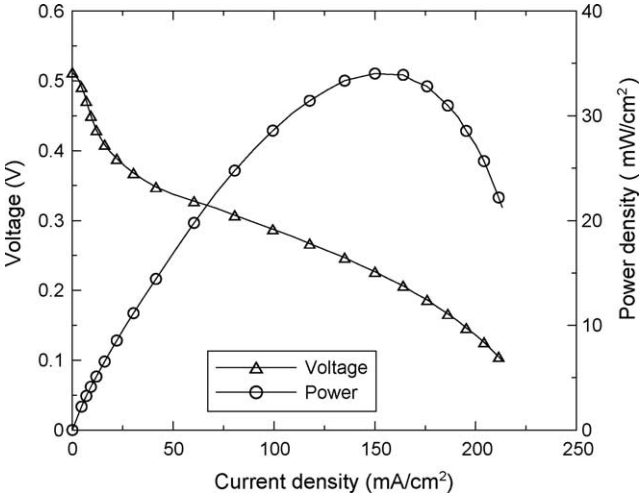

Fig. 1. Polarization curve using 2 M methanol solution at 22 °C, with air flow rate of 161 mL min^{-1}, methanol flow rate of 2.2 mL min^{-1}, and ambient pressure.

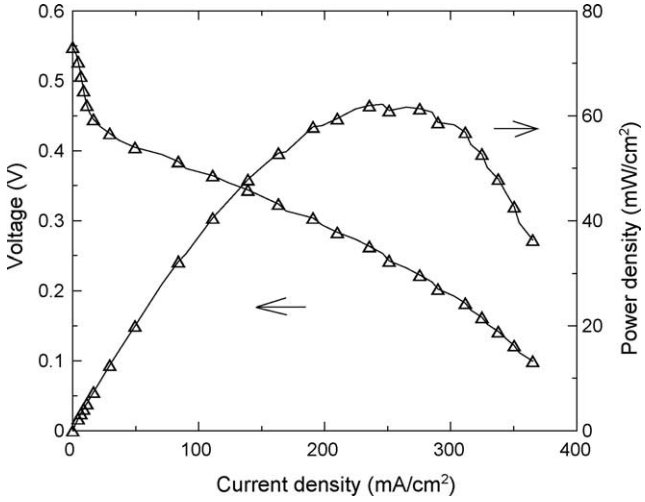

Fig. 2. Polarization curve using 2 M methanol solution at 40 °C, air flow rate of 161 mL min^{-1}, methanol flow rate of 2.2 mL min^{-1}, and ambient pressure.

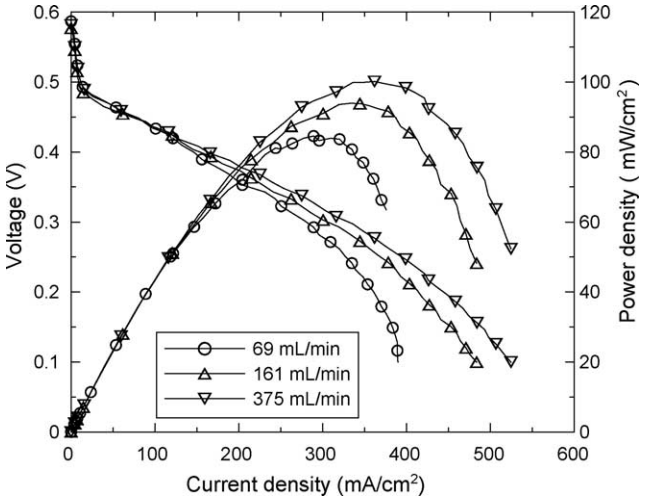

Fig. 3. Polarization curve using 2 M methanol solution at 60 °C at different air flow rates, methanol flow rate of 2.2 mL min^{-1}, and ambient pressure.

lar plates. In the Si-based μDMFC, it was difficult to tighten the cell since the Si wafer is so fragile, making larger contact resistance and less desirable sealing between the MEA and Si wafer. In our previous experiments with the Si-based μDMFC, we found the performance decreased if we further increased the air flow rate in the cathode. This may be caused by cell leakage due to insufficient compression. In contrast, in the present cell using stainless steel plates, the cell performance improves using larger air flow rate, as will be shown shortly.

Fig. 2 depicts the polarization curves and power densities using 2 M methanol solution at 40 °C and atmospheric pressure. The methanol flow rate and the air flow rate are the same as those given in Fig. 1. The cell performance reaches about 200 mA cm^{-2} at 0.3 V and the maximum power density is 62.5 mW cm^{-2} at 0.26 V. This is a significant improvement compared to the previous maximum power density of 33 mW cm^{-2} at 0.17 V in the Si-based μDMFC [6].

Fig. 3 shows the polarization curves and power densities using 2 M methanol solution at 60 °C and atmospheric pressure using different air flow rates. The methanol flow rate was fixed at 2.2 mL min^{-1}. At low current density, the cell voltages are almost identical at different air flow rates. The overall cell performance becomes better with increasing air flow rate. With the air flow rate of 375 mL min^{-1}, cell performance reaches 330 mA cm^{-2} at 0.3 V and the maximum power density is 100.2 mW cm^{-2} at 0.28 V. This is much higher than 50 mW cm^{-2} at 0.2 V and 60 °C for the Si-based μDMFC [6]. Fig. 4 depicts the anode polarization curves when hydrogen gas was fed into the cathode at different temperatures. 2 M methanol solution was used in the anode with the flow rate of 2.2 mL min^{-1}, and the hydrogen flow rate is 161 mL min^{-1} at atmospheric pressure. As expected, the anode overpotential decreases with increased temperature. Using this H_2-evolution counter electrode, the anode overpotential may deviate slightly from that using DHE [19]. However, using the H_2-evolution electrode is still a simple and useful method to evaluate the anode characteristics of a micro cell without a standard reference electrode.

Fig. 5 shows the *I–V* curve when air was replaced by humidified nitrogen in the cathode. The cell fed with nitrogen in the cathode is designed to undergo the charge process. Due to methanol crossover from the anode side to the cathode, the electrochemical reaction in the nitrogen feed side is:

$$CH_3OH + H_2O \rightarrow CO_2 + 6H^+ + 6e^- \quad (1)$$

While on the methanol feed side:

$$6H^+ + 6e^- \rightarrow 3H_2 \quad (2)$$

The methanol crossover rate at open circuit can thus be determined from the limiting current density resulting from transport-controlled methanol oxidation at the nitrogen feed

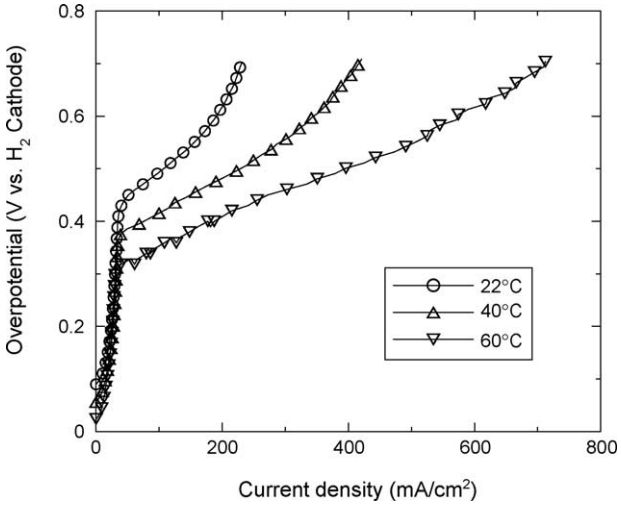

Fig. 4. Anode overpotential with hydrogen cathode, 2 M methanol with flow rate of 2.2 mL min^{-1}, hydrogen flow rate of 161 mL min^{-1}, and ambient pressure.

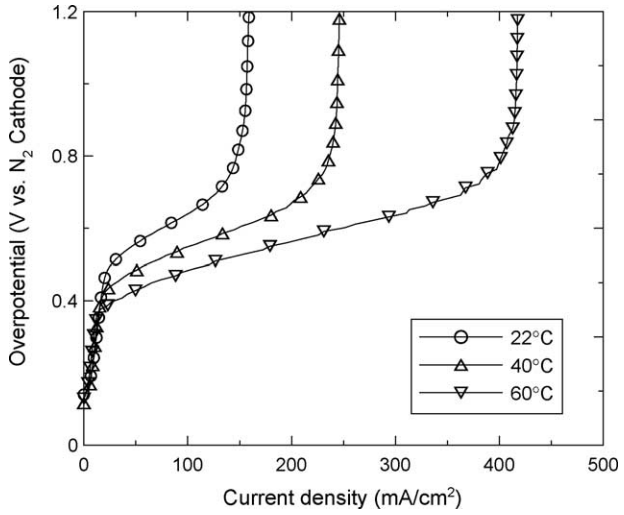

Fig. 5. Methanol crossover rate at open circuit, 2 M methanol with flow rate of 2.2 mL min^{-1}, nitrogen flow rate of 161 mL min^{-1}, and ambient pressure.

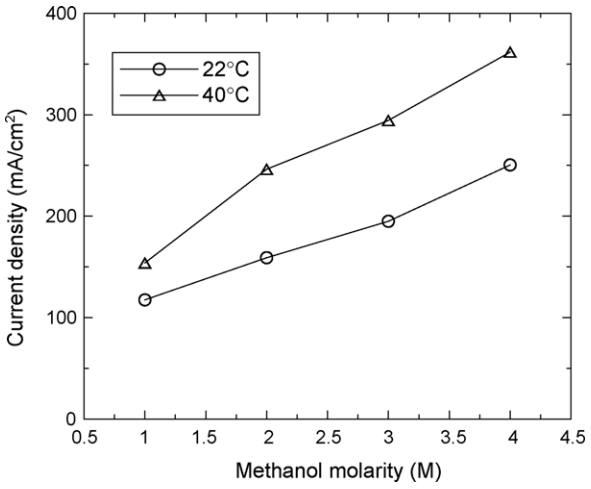

Fig. 6. Methanol crossover rate at open circuit at different molarities, air flow rate of 161 mL min^{-1}, methanol flow rate of 2.2 mL min^{-1}, and ambient pressure.

side [19]. Although the limiting current density may be slightly lower than the methanol crossover rate at OCV due to the effect of electro-osmotic drag of fluid by the protonic current [19], we neglect this effect here for simplicity. From the limiting current density at different temperature shown in Fig. 5, we obtain the methanol crossover rates at OCV for 2 M methanol feeding of 159 mA cm^{-2} at 22 °C, 246 mA cm^{-2} at 40 °C, and 417 mA cm^{-2} at 60 °C. These methanol crossover rates are relatively large for this 1.625 cm^2 DMFC. Using exactly the same MEA, however, with an effective area of 5 cm^2, we assembled a 5 cm^2 graphite cell. Its methanol crossover rates at OCV for 2 M methanol feeding are 103 mA cm^{-2} at 22 °C and 240 mA cm^{-2} at 60 °C, much lower than the crossover rates in the 1.625 cm^2 DMFC cell (i.e., reduced by 35% for 22 °C and 41% at 60 °C). The discrepancy in the crossover rate between the two cells of different size may possibly be attributed to the different ratios of the perimeter to the effective area of the MEAs. This ratio for the 1.625 cm^2 cell is 43% larger than that of the 5 cm^2 cell. On the other hand, the methanol crossover rate will be very large along the peripheral area outside of the effective area of the MEA because there are no resistive layers attached to the membrane such as gas diffusion layer, micro porous layer and catalyst layer. Although we used gasket for fluid sealing, there was still a tolerance gap between the gasket and the diffusion layer, and this gap may provide a shortcut for methanol crossing directly through the thin Nafion® 112 membrane. With a larger ratio of the perimeter to the effective area for the small cell, there is the larger methanol crossover rate per effective area. In conclusion, it is extremely important to carefully seal the gap between the gasket and the diffusion layer in micro DMFCs to decrease the overall methanol crossover rate. Other method for decreasing the methanol crossover rate includes using low flow rate in the anode.

In general, the methanol crossover current density can be mathematically expressed by a simple relation between the crossover current (I_c) and anode mass-transport limiting current density ($I_{A,lim}$) [20]. That is:

$$I_c = I_{c,oc}\left(1 - \frac{I}{I_{A,lim}}\right) \quad (3)$$

where $I_{c,oc}$ is the crossover current density at open circuit, and I is the operating current density. The fuel efficiency (η_{fuel}) taking methanol crossover into account, can be defined as:

$$\eta = \frac{I}{I + I_c} \quad (4)$$

At open circuit ($I = 0$), $\eta_{fuel} = 0$. The fuel efficiency increases with the increasing operating current density. If the operating current density were 250 mA cm^{-2} at 40 °C, since the limiting current density was around 380 mA cm^{-2} shown in Fig. 2 and the crossover rate at OCV was 246 mA cm^{-2} shown in Fig. 5, the fuel efficiency would be 75% according to Eqs. (3) and (4).

Fig. 6 shows the methanol crossover rates at OCV at different molarities and temperatures. The crossover rate at OCV was measured by the same method explained in Fig. 5. For both temperatures of 22 and 40 °C, the crossover rates almost linearly increase with the methanol concentration, and the higher temperature leads to a higher methanol crossover rate, as expected. Fig. 7 shows the effect of the air flow rates on the maximum power density using different methanol solutions at 22 °C. The methanol flow rate was fixed at 2.2 mL min^{-1}. The maximum power density was obtained by scanning the polarization curve. For 1 M methanol solution, there is no significant change of the maximum power density for different air flow rates. However, the maximum power density is much lower than those of concentrated solutions (2–4 M) at the larger air flow rate, which is mainly due to large anode overpotential using dilute methanol solution. The anode overpotential was measured by the method explained in Fig. 4. For the concentrated methanol solution such as 4 M, the max-

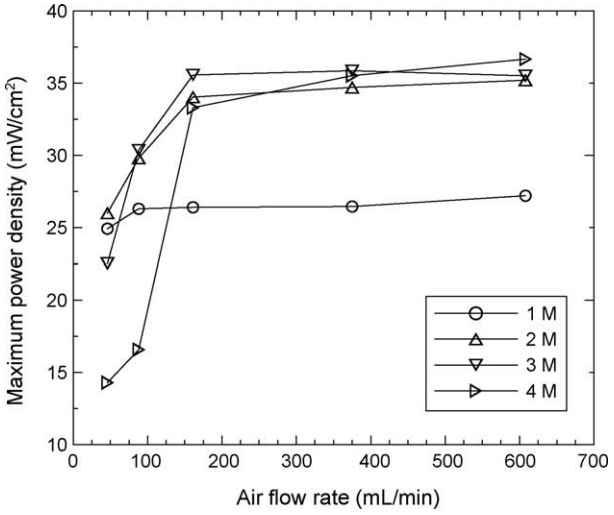

Fig. 7. Maximum power density at different air flow rates, methanol flow rate of 2.2 mL min^{-1}, 22 °C, and ambient pressure.

imum power density changes noticeably at the low flow rate, as shown in Fig. 7, while maximum power density reaches stability at the large air flow rate. Fig. 8 shows the maximum power density changes with air flow rate at 40 °C and atmospheric pressure. Similar to the case at 22 °C, the maximum power density varies noticeably at the low air flow rates for 2–4 M methanol solutions, while eventually the maximum power density converges at high air flow rates. We believe that the low performance at small air flow rates is due to the mass transport limitation of the thick Toray carbon paper GDL. An additional experiment in an air-breathing DMFC cell (not shown here) comparing the mass transport phenomena in Toray carbon paper and E-tek carbon cloth as different GDLs while all other conditions remain the same reveals that the MEA with carbon cloth for the cathode GDL produces much higher performance at small air flow rate.

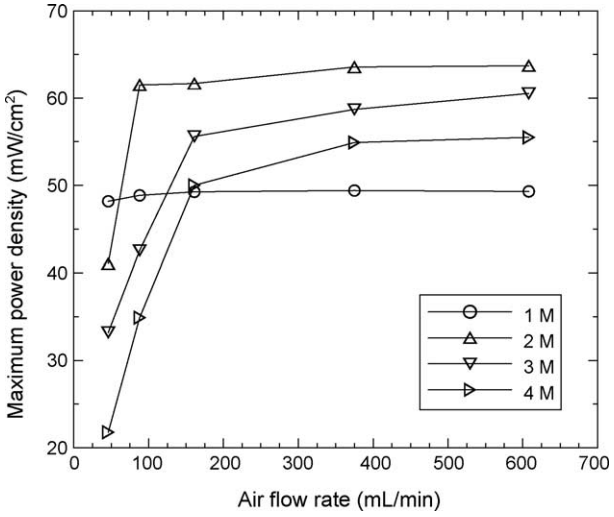

Fig. 8. Maximum power density at different air flow rates, methanol flow rate of 2.2 mL min^{-1}, 40 °C, and ambient pressure.

4. Conclusion

A μDMFC with an active area of 1.625 cm^2 has been developed. The flow channels were fabricated on stainless steel plates using a photochemical etching method. The maximum power density reaches 62.5 mW cm^{-2} at 40 °C and 100 mW cm^{-2} at 60 °C using 2 M methanol solution under ambient pressure, which was almost double our previous results with a Si-based μDMFC. In addition, it was found that the methanol crossover rate depends on the effective area of the MEA. Furthermore, it was pointed out that the large mass transport capability of a cathode GDL is necessary for high performance with the cell operating at a low air stoichiometry. The results presented in this paper should be useful for the development of high-power μDMFCs for portable application.

Acknowledgment

This work was supported by DARPA Microsystem Technology Office (MTO) under contract no. DAAH01-1-R001.

References

[1] S.R. Narayanan, T.I. Valdez, in: Wolf Vielstich, Arnold Lamm, Hubert A. Gasteiger (Eds.), Handbook of Fuel Cells, Fundamental, Technology and Application, 4, John Wiley & Sons, 2003, p. 1133.
[2] X. Ren, T.E. Springer, T.A. Zawodzinski, S. Gottesfeld, J. Electrochem. Soc. 147 (2000) 466.
[3] A.S. Arico, S. Srinivasan, V. Antonucci, Fuel Cells 1 (2001) 133.
[4] A.K. Shukla, C.L. Jackson, K. Scott, R.K. Raman, Electrochim. Acta 47 (2002) 3401.
[5] C.K. Dyer, J. Power Sources 106 (2002) 31.
[6] G.Q. Lu, C.Y. Wang, T.J. Yen, X. Zhang, Electrochim. Acta 49 (2004) 821.
[7] T.J. Yen, N. Fang, X. Zhang, G.Q. Lu, C.Y. Wang, Appl. Phys. Lett. 83 (2003) 4056.
[8] S.C. Kelley, G.A. Deluga, W.H. Smyrl, Electrochem. Solid State 3 (2000) 407.
[9] S.C. Kelley, G.A. Deluga, W.H. Smyrl, AICHE J. 48 (2002) 1071.
[10] N. Mano, A. Heller, J. Electrochem. Soc. 150 (2003) A1136.
[11] H.H. Kim, N. Mano, X.C. Zhang, et al., J. Electrochem. Soc. 150 (2003) A209.
[12] S.J. Lee, A. Chang-Chien, S.W. Cha, R. O'Hayre, Y.I. Park, Y. Saito, F.B. Prinz, J. Power Sources 112 (2002) 410.
[13] H.L. Maynard, J.P. Meyers, J. Vac. Sci. Technol. B 20 (2002) 1287.
[14] A. Heinzel, C. Hebling, M. Muller, M. Zedda, C. Muller, J. Power Sources 105 (2002) 250.
[15] J.R. Yu, P. Cheng, Z.Q. Ma, B.L. Yi, Electrochim. Acta 48 (2003) 1537.
[16] J.R. Yu, P. Cheng, Z.Q. Ma, B.L. Yi, J. Power Sources 124 (1) (2003) 40.
[17] J. Pavio, J. Bostaph, A. Fisher, J. Hallmark, B.J. Mylan, C.G. Xie, Adv. Microelectron. 29 (2002) 1.
[18] C. Lim, C.Y. Wang, J. Power Sources 113 (2003) 145.
[19] X. Ren, T.E. Springer, S. Gottesfeld, J. Electrochem. Soc. 147 (2000) 92.
[20] G.Q. Lu, F.Q. Liu, C.Y. Wang, Electrochem. Solid State Lett. 8 (2005) A1.